Iron Wheels on Silicon: Wetting Behavior and Electronic Structure of Adsorbed Organostannoxane Clusters

F. Frehill,[†] K. H. G. Schulte,[‡] C. P. Martin,[‡] L. Wang,[‡] S. Patel,[§] J. A. Purton,[§] J. G. Vos,[†] and P. Moriarty*[,‡]

National Centre for Sensor Research and School of Chemical Sciences, Dublin City University, Glasnevin, Dublin 9, Ireland, School of Physics & Astronomy, University of Nottingham, Nottingham NG7 2RD, UK, and Daresbury Laboratory, Daresbury, Cheshire WXX 4AD, UK

Received December 19, 2003. In Final Form: May 12, 2004

Atomic force microscopy and synchrotron radiation (SR) spectroscopy have been used to study the wetting behavior and electronic structure of thin films of a novel organometallic cluster − $[BuSn(O)OC(O)Fc]_6$ ("Fc" = ferrocenyl) − on silicon substrates. This cluster comprises six ferrocene units connected to a stannoxane central core − "an iron wheel on a tin drum" (V. Chandrasekhar; et al. *Angew. Chem., Int. Ed.* **2000**, *39*, 1833). Thin films spin-cast onto native oxide-terminated silicon readily dewet the substrate. We have utilized advanced image analysis techniques based on Minkowski functionals to provide a detailed quantitative analysis of the morphology of the stannoxane overlayers. This analysis shows that the dewetting patterns are rather far removed from those expected to arise from a simple Poisson distribution of centers, and we discuss the implications of this finding in terms of nucleated and spinodal dewetting. Variations in both the surface roughness and the in-plane correlation length have been followed as a function of annealing time to probe the surface dewetting dynamics. SR valence band photoemission illustrates that the highest occupied molecular orbital (HOMO) of the cluster is found 2 eV below the Fermi level. Fe 2p → 3d and Sn 3d → 5p resonant photoemission spectroscopy have been used to enhance the cross sections of the partial density of states associated with the Fe and Sn atoms. Sn atoms make a large contribution to the HOMO of the cluster, whereas the Fe atoms are associated with an electronic environment seemingly very similar to that in the "parent" ferrocene molecule.

I. Introduction

Organometallic chemistry underlies the synthesis and functionality of a wide variety of molecular and polymeric systems. Metallocenes, and ferrocene[1] in particular, have been exploited as central elements of a family of nascent molecular electronics devices. These prototype systems include components whose structure or conformation is switchable via variations in redox state,[2] and a variety of switching methods have been envisaged. For example, magnetic control of the activity of (bio)electrocatalytic systems has recently been demonstrated by Katz et al.,[3] photoisomerization has been exploited by a number of groups[4,5] to generate redox-active states, and variations in pH are commonly used to reversibly modify molecular properties.[6]

The synthesis of the organometallic molecule of interest in this study, $[BuSn(O)OC(O)Fc]_6$ (where "Fc" = ferrocenyl), was first reported by Chandrasekhar et al. three years ago.[7] The molecule comprises six ferrocene units which are attached to a central stannoxane core. As discussed in ref 7, this represents a rather novel cyclic interconnection of Fc elements. In more recent work,[8] Chandrasekhar et al. have shown that it is possible to generate supramolecular "grids" of the stannoxane cluster through the formation of intermolecular C−H--O bonds between the ferrocenyl C−H and the carboxylate oxygen. This is an exciting development as it provides a relatively simple route, via the formation of hydrogen bonds, to the self-assembly of ferrocene−stannoxane clusters into a predefined pattern in the solid state.

A key motivation underlying the work described in this paper relates to the possibility of ultimately translating the supramolecular chemistry and crystal engineering described above to the self-assembly of organostannoxane (and other organometallic) clusters on a solid surface. This is a goal that has parallels in many areas of state-of-the-art nanoscale science. For example, alongside the development of synthetic procedures that impart device-related functionality to single molecules, there has been a drive toward the integration of molecular electronics with more conventional silicon technology.[9] There are many scientific issues to address in this area with some of the more fundamental questions related to the manner in which the molecular units interact with a substrate. Although considerable effort has been expended in studying the interaction of a range of small organic molecules with atomically clean, reconstructed silicon surfaces under ultrahigh vaccum (UHV) conditions,[10−12] many applications necessitate an understanding of the self-organization, interactions, and morphology of molecular and polymeric systems deposited from solution. It is important

[†] Dublin City University.
[‡] University of Nottingham.
[§] Daresbury Laboratory.

(1) Special edition on ferrocene chemistry. *J. Organomet. Chem.* **2001**, *637−639*.
(2) Plenio, H.; Aberle, C. *Chem.-Eur. J.* **2001**, *7*, 4438.
(3) Katz, E.; Sheeney-Haj-Ichia, L.; Willner, I. *Chem.-Eur. J.* **2002**, *8*, 4138.
(4) Tsivgoulis, G. M.; Lehn, J.-M. *Adv. Mater.* **1997**, *9*, 39.
(5) Takeshita, M.; Choi, C. N.; Irie, M. *Chem. Commun.* **1997**, 2265.
(6) Bissell, R. A.; Cordova, E.; Keifer, A. E.; Stoddard, J. F. *Nature* **1994**, *369*, 133.
(7) Chandrasekhar, V.; Nagendran, S.; Bsal, S.; Kozec, M. A.; Powell, D. R. *Angew. Chem., Int. Ed.* **2000**, *39*, 1833.
(8) Chandrasekhar, V.; Boomishankar, R.; Singh, S.; Steiner, A.; Zacchini, S. *Organometallics* **2002**, *21*, 4575.
(9) Fang, L. A.; Liu, J. M.; Coulter, S.; Cao, X. P.; Schwartz, M. P.; Hacker, C.; Hamers, R. J. *Surf. Sci.* **2002**, *514*, 362.
(10) Schwartz, M. P.; Hamers, R. J. *Surf. Sci.* **2002**, *515*, 75.
(11) Cao, X. P.; Hamers, R. J. *J. Am. Chem. Soc.* **2001**, *123*, 10988.
(12) Lopinski, G. P.; Wayner, D. D. M.; Wolkow, R. A. *Nature* **2000**, *406*, 48.

10.1021/la036414y CCC: $27.50
Published on Web 06/22/2004

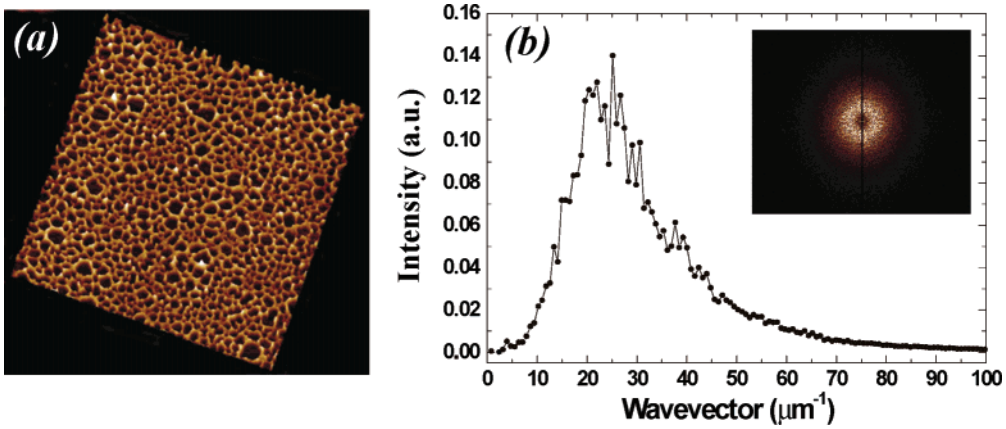

Figure 1. (a) Tapping mode atomic force microscope (AFM) image (8 μm × 8 μm) of a thin stannoxane film spin-cast from toluene onto a native-oxide-terminated Si(111) substrate. The film has a cellular morphology with a mean thickness of ~4 nm. The dewetting holes in the film expose the underlying SiO_2/Si substrate. (b) A radial average of a 2D Fourier transform (FT) of the image shown in (a). The 2D FT is shown in the inset. Note the presence of a peak at a wavevector, q, of ~25 μm^{-1}, suggesting the presence of an intercell correlation length of ~$2\pi/25$ μm (i.e., ~250 nm). Note that the somewhat poor statistics associated with the radially averaged Fourier transforms shown throughout this paper arise from the relatively small scan area (and thus small number of cells) associated with each image.

to establish if the resulting (spin-cast or drop-deposited) thin film is stable, unstable, or metastable and the extent to which it will dewet the underlying substrate/electrode surface.

The issue of wettability is of paramount importance when considering the possibility of hydrogen-bonding-mediated self-assembly of 2D organostannoxane (or other organometallic) overlayers. Hence, the first component of the Results section below details a study of the dewetting of spin-cast organostannoxane thin films on native oxide-terminated silicon substrates. A particular goal of our work was to probe whether organostannoxane thin films on silicon are subject to the spinodal dewetting[13] mechanism that has been shown to drive the break-up of liquid crystal,[14] homopolymer,[15] and, most recently, copolymer[16] films on silicon substrates. As discussed by Brochard-Wyart and Dallinat[13] and Reiter,[17] spinodal dewetting involves the amplification of thin film thickness fluctuations via long range van der Waals forces and leads to the break-up of an adsorbed molecular film. This mode of dewetting is distinctly different from the thermal or heterogeneous nucleation of holes in a metastable film and is analogous to spinodal decomposition in fluid mixtures where the thickness fluctuations correspond to composition fluctuations in the fluid system. A key feature of both spinodal decomposition and spinodal dewetting is the presence of a preferred length scale in the phase separation/film rupture process. (As discussed in section III, however, a spinodal mechanism is not always necessary to account for spatial correlations in the positions of dewetting centers.) The presence of a dominant length scale has considerable implications for controlled self-assembly, and, indeed, spinodal processes have been exploited by a number of groups in the synthesis of a variety of nanoscale patterns in polymer layers.[18] However, to date, there is a paucity of literature on the dewetting of nonpolymeric adsorbed layers on silicon.

The second component of the Results section deals with the solid-state electronic structure of the organostannoxane cluster used in this work as was probed using synchrotron radiation photoemission and resonant photoemission (RESPES). Resonant photoemission, in particular, is a sensitive probe of the density of states associated with the Fe and Sn atoms at the core of the stannoxane and ferrocenyl units.

II. Experimental Section

The organostannoxane cluster used throughout this work was synthesized via the procedure described in ref 7. Briefly, *n*-butylstannonic acid is reacted with ferrocene monocarboxylic acid in benzene to yield the hexaferrocene−stannoxane compound via reaction 1 below:

$$6\mathrm{BuSn(O)OH} + 6\mathrm{FcCOOH} \xrightarrow[80\ ^\circ\mathrm{C}]{\mathrm{C_6H_6}} [\mathrm{[BuSn(O)OC(O)Fc]_6}] + 6\mathrm{H_2O} \quad (1)$$

where, again, "Fc" represents a ferrocenyl moiety. Chandrasekhar et al.[7] point out that not only is reaction 1 important in that it produces a hexaferrocene compound in high yield (as compared to the modest yields of multiferrocene compounds produced via other synthetic routes), but the resulting hexaferrocene−stannoxane cluster is robust and thermally stable up to temperatures of 244 °C.

For both the atomic force microscopy (AFM) and the SR spectroscopy measurements detailed in sections III.A and III.B below, thin films were prepared by spin-coating (at 4 krpm) 15 μL of a 0.25 mM solution of the organostannoxane cluster in toluene onto a 0.7 cm^2 piece of a native oxide-covered Si(111) sample. For the SR measurements, the silicon samples were simply solvent-rinsed and blow-dried with N_2 before spin-coating. However, for the AFM measurements, where the wetting properties of the molecules were of interest, in addition to solvent-cleaned substrates, we used samples which were subsequently further cleaned with a 1:1 mixture of H_2SO_4:H_2O_2 (30%) for 1 h. These were then thoroughly rinsed with deionized water. This surface treatment strongly improved the reproducibility of the organostannoxane film morphology from sample to sample. Furthermore, dynamic contact angle measurements showed that the wetting properties of the Si substrate were dramatically affected by the H_2SO_4:H_2O_2 treatment. For solvent-rinsed samples, the contact angle was 45° ± 5°, whereas the sulfuric acid−peroxide treatment dramatically reduced the hydrophobicity of the surface so that the contact angle was 5° ± 5°.

(13) Brochart-Wyatt, F.; Dalliant, J. *Can. J. Phys.* **1990**, *68*, 1084.
(14) Herminghaus, S.; Jacobs, K.; Mecke, K.; Bischof, J.; Fery, A.; Ibn-Elhaj, M.; Schlagowski, S. *Science* **1998**, *282*, 916.
(15) Thiele, U.; Velarde, M. G.; Neuffer, K. *Phys. Rev. Lett.* **2001**, *87*, 016104.
(16) Müller-Buschbaum, P.; Wolkenhauer, M.; Wunnicke, O.; Stamm, M.; Cubitt, R.; Petry, W. *Langmuir* **2001**, *17*, 5567.
(17) Reiter, G. *Phys. Rev. Lett.* **1992**, *68*, 75.
(18) Higgins, A. M.; Jones, R. A. L. *Nature* **2000**, *404*, 476.

SR photoemission and RESPES measurements were taken on Beamline 5U1 of the UK Synchrotron Radiation Source (SRS) at Daresbury. The photon energy range of this undulator beamline is 60 eV to 1 keV. Photon energies were calibrated using Ti L_2 X-ray absorption spectra from a TiO_2 thin film (that could be moved into and out of the beam "upstream" from the sample) and Si $L_{2,3}$ edge spectra from the silicon substrate. A VSW HA100 hemispherical electron energy analyzer with single channel detection was used for all photoemission and resonant photoemission (RESPES) measurements. All photoelectron binding energies were calibrated by referencing to the Si 2p photoemission peak (at a binding energy of 99.5 eV) of the native oxide-terminated Si(111) substrate.

III. Results and Discussion

A. Wetting and Dewetting of Organostannoxane Thin Films. Thin adsorbed films play a central role in processes and applications ranging from protective/lubricating coatings to optoelectronic device technology to the functionalization of solid surfaces for biomedical applications. Thin film stability is therefore an issue of far-reaching scientific significance. In terms of the organostannoxane films of interest in this paper, a number of important questions needed to be addressed: (i) Do stannoxane films wet silicon? (ii) What type of film morphology results from spin-coating? (iii) If the films are unstable or metastable, is the dewetting mechanism related to "conventional" nucleation and spreading of holes, or is a spinodal process (giving rise to spatially correlated morphological features) involved? A detailed AFM study (with subsequent quantitative image analysis) of as-prepared and annealed spin-cast organostannoxane thin films has been carried out to address these issues.

Figure 1a is an AFM image of an organostannoxane film spin-cast onto a Si substrate which was simply solvent-cleaned and dried with N_2. Note that even before the sample is annealed, the stannoxane overlayer adopts a cellular morphology. As discussed by a number of authors,[15,17] the cellular network structure arises from the coalescence of the rims of expanding dewetting holes. However, one must distinguish between dewetting processes derived from an intrinsic surface instability (i.e., spinodal dewetting) and heterogeneous or thermal nucleation mechanisms. An important characteristic of spinodal dewetting is that the positions of the dewetting holes should be strongly spatially correlated as a result of the critical wavevector associated with the instability.[13] For a nucleation mechanism, the spatial correlation is absent, and the hole positions should follow a Poisson distribution. (However − and importantly − see the discussion regarding hole coalescence below.)

As a first step in the determination of the degree of interhole correlation, the Fourier transform (FT) of the image may be examined for the presence of a preferred wavevector. As shown in the inset to Figure 1b, a distinct ring is observed in the two-dimensional FT. Similarly, a clear peak appears in the radially averaged transform (Figure 1b). This is already strong evidence for spatial correlations in the hole positions. However, to provide a more quantitative distinction between correlated and uncorrelated dewetting centers, we have adopted a powerful statistical geometry technique based on Minkowski functionals[19] and previously applied by Jacobs et al.[20] to dewetting patterns.

Minkowski functionals are related to important morphological measures. In two dimensions, these are the covered area, boundary length, and Euler characteristic of the pattern of interest.[21] While the covered area and perimeter length are easy-to-visualize geometrical quantities, the third Minkowski measure − the Euler characteristic, χ − is perhaps not encountered so frequently and merits a brief explanation. χ is a key topological measure describing the connectivity of a pattern. In two dimensions − and on a binary image consisting of black and white pixels − the Euler characteristic is the number of separate objects comprising interconnected black pixels minus the number of enclosed white regions.[21]

Using an efficient algorithm based on that put forward by Michielsen and Raedt,[21] we have calculated[22] the behavior of the morphological Minkowski measures for a 2D distribution of points whose coordinates are given by the centers of the cells shown in Figure 1a. Specifically, to determine the degree to which the cell centers in Figure 1a deviate from the Poisson distribution of points expected from a conventional nucleation-driven dewetting scenario, we have adopted the following procedure. To each "germ" (i.e., cell center − see inset to Figure 2a) which has an edge length of 1, we attach a square "grain" of edge length $2r + 1$ (where r is a positive integer whose initial value is 1). Thus, and as described in detail by Michielsen and Raedt,[21] the point pattern arising from the cell centers is transformed into a pattern of square grains. We now systematically vary the grain size r − or, as in Figure 2, the "normalized" quantity $x = r/L$, where L is the mean germ separation − and compare the changes in the three Minkowski functionals (see Figure 2) to those expected for a Poisson distribution.

Considering first the x-dependent variation in Minkowski functionals for a Poisson distribution of points (represented by the solid lines in Figure 2a−c), we note that for small x, the grains are isolated. This produces a small covered area, a small boundary length, and a positive Euler characteristic. As the grain size is increased, the degree of overlap rises in a characteristic manner until the entire 2D plane is covered with black pixels producing a "saturated" covered area (Figure 2a). The boundary length curve exhibits a clear peak (Figure 2b) at intermediate values of x, while the Euler characteristic turns negative (Figure 2c). The minimum in the Euler characteristic curve (Figure 2c) arises from the highly interconnected and "void-ridden" structure present at intermediate x values.

The x-dependent behavior of the Minkowski functionals for the distribution of points with coordinates given by the cell centers in Figure 1a is markedly different. In each case − area, perimeter, and Euler characteristic − the curve for the stannoxane film centers (open circles-solid lines in Figure 2a−c) deviates significantly from that for the Poisson distribution. It is particularly interesting to note that the Euler characteristic decreases much more rapidly for a Poisson distribution at low values of x than for the distribution of points derived from the dewetting centers in the stannoxane film. To highlight more clearly the deviations from a Poisson distribution, Figure 2d−f shows graphs of the stannoxane film-related Minkowski functionals minus the corresponding Poisson-derived functional. That the distribution of dewetting centers in the stannoxane film is far removed from that expected for a Poisson distribution of points is clear from these graphs.

(19) Stoyan, D.; Kendall, W. S.; Mecke, J. *Stochastic Geometry and its Applications*; Akademie Verlag: Berlin, 1989.

(20) Jacobs, K.; Herminghaus, S.; Mecke, K. R. *Langmuir* **1998**, *14*, 965.

(21) Michielsen, K.; De Raedt, H. *Comput. Phys. Commun.* **2000**, *132*, 94.

(22) The code to numerically calculate the 2D Minkowski functionals was written in Matlab and is available from C. P. Martin (ppxcpm1@nottingham.ac.uk).

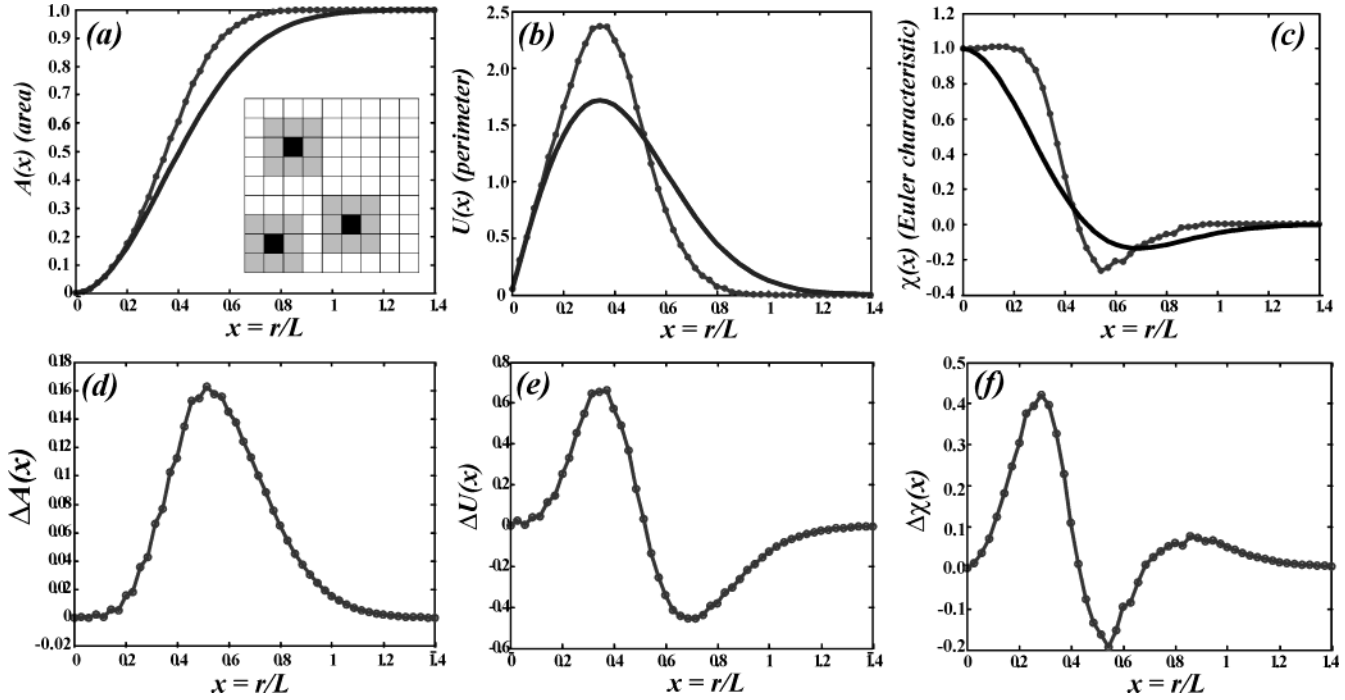

Figure 2. (a−c) Minkowski functionals (covered area, boundary length, and Euler characteristic) for a Poisson distribution of points and a point set based on the coordinates of the dewetting cell centers for the image shown in Figure 1 (solid lines and filled circles/solid lines, respectively). In each case, the functionals are plotted as a function of x, the normalized grain size. The inset to (a) depicts the difference between germs (the black pixels) and grains (grey pixels) centered on the germs. Note the strong deviation of each of the Minkowski functionals for the stannoxane-derived point system from the functionals for a Poisson-distributed set of points. (d−f) Difference between the stannoxane- and Poisson-derived result for each 2D Minkowski functional.

One might now argue that as the spatial distribution of the dewetting centers does not follow a Poisson distribution, there is clear evidence for spinodal dewetting of the organostannoxane film. However, a number of groups[23] have recently pointed out that for the "inverse" problem of droplet (rather than hole) growth on a substrate, deviation from a nonrandom spatial distribution of domains can occur simply by the coalescence of close pairs of droplets. Coalescence "wipes out" the clustering inherent in a Poisson point distribution and introduces a minimum nearest-neighbor distance. This, in turn, produces a spatial correlation length in the droplet − or, in our case, hole − distribution. More detailed morphological comparisons of dewetting center distributions, coupled with simulation studies, are required to address this issue and are underway in our group.

It is important to highlight at this point that the organostannoxane films we have studied have been produced via spin-coating. This is an exceptionally complicated, far-from-equilibrium process that has been considered by Lawerence[24] (among others) to comprise three consecutive phases. Following the initial transient phase where fluid inertia, the Coriolis force, and surface tension are the dominant effects, the second phase of the process involves a balance between viscous and centrifugal forces. In this secondary phase, the dynamics are driven by fluid flow, whereas in the final phase (phase III), the fluid viscosity is so high the evolution of the film is largely driven by solvent evaporation. Unfortunately, our AFM measurements − which provide little or no information on the film growth dynamics − cannot address the question of whether the viscosity of the fluid plays a large role in defining the final film morphology we observe. While one might speculate that the absence of macroscopic spatial uniformity in the organostannoxane films suggests that phase II dynamics are important, we do not observe a "starlike" pattern (previously identified as the signature of hydrodynamic instabilities[25]) at the center of rotation. An optical scattering study may provide some insight into the influence of the spin-coating process on the film morphology.

Having quantitatively ascertained that the morphology of as-cast stannoxane films on native oxide-terminated Si(111) substrates is primarily determined by the presence of a well-defined correlation (but not necessarily spinodal) wavelength, we now consider the dynamics of dewetting. We have carried out a comprehensive series of annealing studies of stannoxane thin films on (both H_2SO_4:H_2O_2-treated and "out of the box" solvent-rinsed) silicon samples to probe whether the evolution of the film morphology is consistent with models of spinodal dewetting. As described below, within the range of annealing times and annealing temperatures used in our study (30 min to 60 h, 75− 125 °C) and for organostannoxane films ranging in thickness from ∼4 to 10 nm (on H_2SO_4:H_2O_2-treated silicon), we find no consistent evidence for the evolution of surface wavevector expected from the theory of spinodal dewetting. We also see considerable differences in the annealing-induced morphological evolution for stannoxane films on H_2SO_4:H_2O_2-treated silicon as compared to Si(111) substrates which have simply been solvent-rinsed. We return to this important point below.

Brochard and Dalliant[13] have put forward a variant of Vrij's[26] original capillary wave instability model to treat spinodal dewtting of thin liquid films from solid substrates. Both the Brochard and Dalliant and the Vrij models predict that thickness fluctuations of the film can be approximated by the following expression:

$$z(x,t) = h + \delta h e^{iqx}$$

Here, the fluctuation amplitude, δh, is given by: $\delta h =$

(23) Brinkmann, M. *Phys. Rev. B* **2002**, *66*, 165430. Ruckenstein, E.; Dadyburjor, D. B. *Thin Solid Films* **1978**, *55*, 89.
(24) Lawrence, C. J. *Phys. Fluids* **1988**, *31*, 2786.

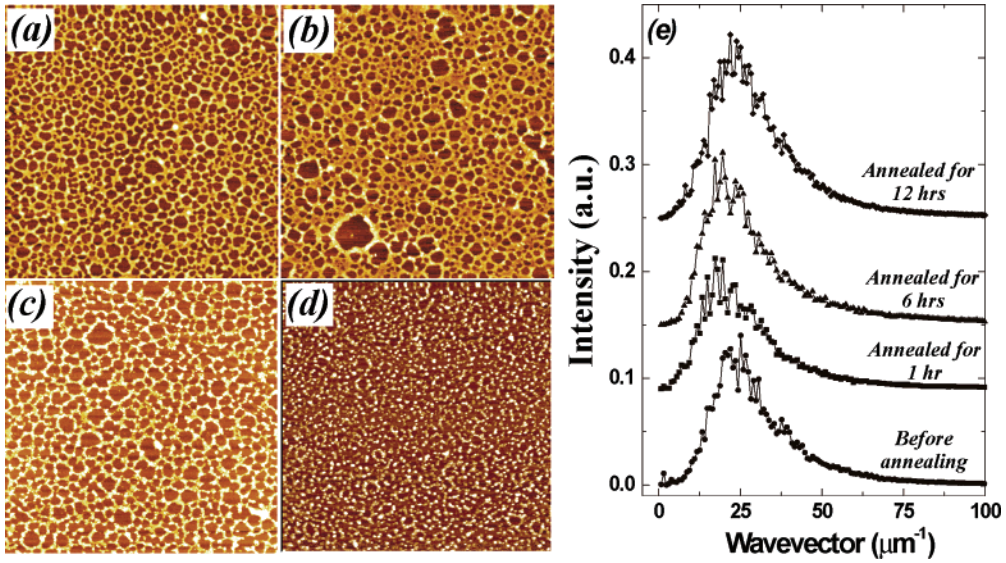

Figure 3. (a−d) 8 μm × 8 μm AFM images for a stannoxane thin film annealed for progressively longer times at a temperature of 75 °C. (a) is a "plan view" representation of the image shown in Figure 1a and illustrates the morphology of the film directly following spin-casting with no annealing. (b−d) are AFM images taken following annealing periods of 1, 6, and 12 h, respectively. It is important to note that, although these images are largely representative of the macroscopic morphology of the film, as described in the text, variations in roughness and peak wavevector were observed at different regions across the film. The progressive break-up of the film (via the Rayleigh instability) into droplets is clear from the images (although following 12 h of annealing, an "imprint" of the original cellular structure remains − cf. Figure 5d). (e) Radially averaged 2D FTs for the images shown in (a−d). From bottom to top: before annealing, following 1 h of annealing, following 6 h of annealing, following 12 h of annealing.

$\delta h_0 e^{t/\tau}$, where τ is the relaxation time (and $1/\tau$ is the growth rate), and δh_0 is the initial fluctuation amplitude. The x coordinate is associated with displacements parallel to the surface, and q denotes the wavevector associated with the wave instability. In this model, thermally driven thickness fluctuations are exponentially amplified if their associated wavevector (q) is less than some critical wavevector, q_C, but are attenuated if $q > q_C$. Importantly, if one now monitors the distribution of wavevectors by, for example, plotting the radially averaged Fourier transform of AFM images of the thin film taken as a function of annealing time, then it is possible to determine a value for q_C by identifying a "crossover" wavevector in the Fourier spectra. Furthermore, the position of the peak in the radially averaged transform shifts to lower wavenumbers as a function of annealing time according to a power law whose exponent yields information on the type of underlying destabilization kinetics. These types of analyses have been successfully adopted by Xie et al.[27] (among others) in the analysis of dewetting of polymer films from silicon substrates.

Figure 3a−d is a series of representative AFM images for a stannoxane film annealed for progressively longer times at a temperature of 75 °C. We have measured the in-plane peak wavevector as a function of annealing time by acquiring similar AFM images at a number of well-separated regions (spaced by millimeters) on the stannoxane film and subsequently calculating the radially averaged Fourier transform. Figure 3e shows the corresponding radially averaged Fourier transforms for Figure 3a−d. As shown in the inset to Figure 4, within the range of annealing times and error limits associated with our study, we do not recover the power-law dependence of wavevector on annealing time which has previously been observed in studies of polymer dewetting from silicon

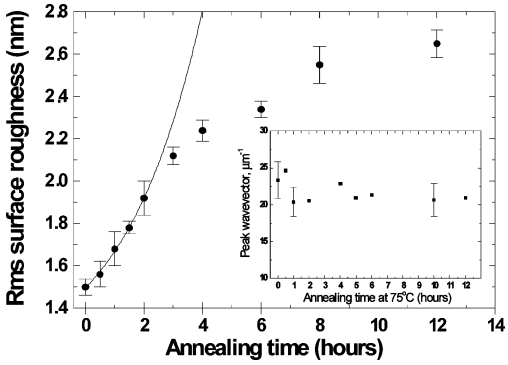

Figure 4. Evolution of surface roughness as a function of annealing time. Error bars represent ±1 standard deviation for a set of 30 measurements taken at various macroscopically separated regions of the film. Although it is possible to fit the early stage annealing data with an exponential function (as expected on the basis of the spinodal dewetting theory), the magnitude of the error bars means that a number of other functional forms can also be used as a fit to the data. Inset: Plot of the peak wavevector as a function of annealing times. Representative error bars for a number of points are shown. Within the error limits, we observe no systematic change of the peak wavevector.

substrates.[16,27] Furthermore, from the Fourier transforms of our AFM data (e.g., Figure 3e), it is extremely problematic to systematically and reproducibly define a crossover wavevector (q_c) above (below) which thickness fluctuations decay (grow) in time. These difficulties in interpreting our experimental data in terms of spinodal dewetting theory arise in part from variations in stannoxane film structure from region to region across the substrate sample. Morphological variations across the film substantially increase the magnitude of the error bars (shown as ±1 standard deviation) on the data points and render detailed comparison with theory difficult.[28] However, it is also important to note that the initial (i.e., preannealed) film is associated with a morphology where the dewetting holes already expose the underlying silicon

(25) Müller-Buschbaum, P.; Gutmann, J. S.; Wolkenhauer, M.; Kraus, J.; Stamm, M.; Smilgies, D.; Petry, W. *Macromolecules* **2001**, *34*, 1369.
(26) Vrij, A. *Discuss. Faraday Soc.* **1966**, *42*, 23.
(27) Xie, R.; Karim, A.; Douglas, J. F.; Han, C. C.; Weiss, R. A. *Phys. Rev. Lett.* **1998**, *81*, 1251.

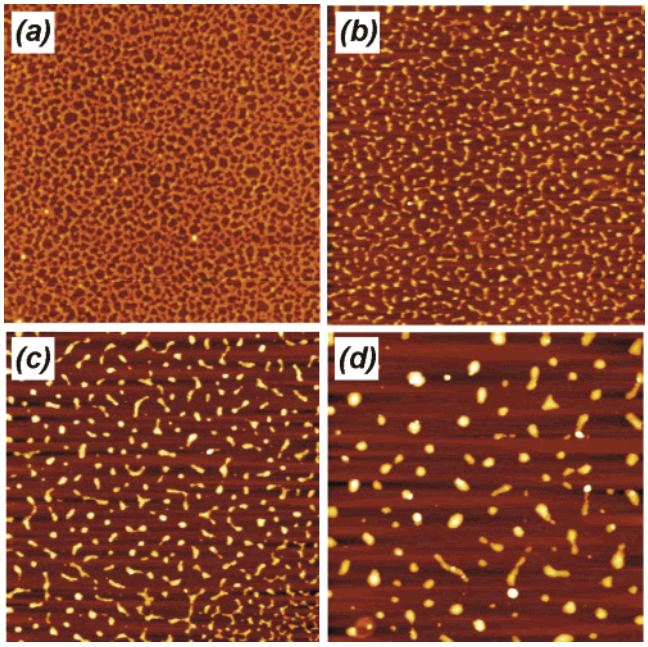

Figure 5. 8 μm × 8 μm AFM images for a stannoxane thin film on a silicon substrate which was simply solvent-rinsed before spin-coating. The evolution of the film as a function of annealing time (again at 75 °C) is markedly different from that observed in Figure 3. (b−d) are images of the film following annealing for 2, 4, and 8 h, respectively. In this case, the film has broken up into well-dispersed droplets following the 8 h of annealing (cf. Figure 3d). Note, however, that the film homogeneity and sample-to-sample reproducibility were substantially poorer for the solvent-rinsed substrates as compared to those substrates which underwent a H_2SO_4:H_2O_2 treatment prior to spin-casting the film.

substrate and the film roughness is rather close to one-half the mean film thickness (2.1 nm). These initial conditions are somewhat different from, for example, previous studies of polymer dewetting from silicon,[27] where the latter criterion was not met until the sample was annealed for some time.

Figure 4 shows the change in surface roughness as a function of annealing time for the stannoxane sample shown in Figures 1 and 3. While it is possible to fit the early stage annealing data (up to ~3 h) with an exponential function − as expected on the basis of spinodal dewetting theory − note again that the error bars are relatively large (and derive once more from morphological variations as a function of lateral position on the sample surface). When coupled with the lack of systematic wavevector variation and the difficulties associated with defining q_c discussed in the previous paragraph, it is clear that, although there is a strong spatial correlation in the positions of the dewetting centers (an important result in itself, given the recent uncertainty regarding spinodal dewetting for adsorbed polymer films on silicon[20]), a quantitative understanding of the dewetting dynamics of the stannoxane film as a function of annealing time is currently lacking.

Further elucidation of the dewetting mechanism will necessitate extremely careful control of substrate heterogeneity and surface chemistry. In particular, substrate surface treatment plays a central role in controlling the dewetting dynamics. Figure 5 shows the evolution of morphology for a film of thickness comparable to that discussed above but spin-cast onto a silicon substrate that was simply solvent treated. It is clear that, although the initial morphology is comparable to that of the H_2SO_4:H_2O_2-treated samples (compare Figure 1a with Figure 5a), the dependence of film morphology on annealing time is dramatically different. In particular, the break-up of the film into droplets via the Rayleigh instability[17,27] occurs on much shorter time scales for the untreated silicon substrate. In addition, sample-to-sample reproducibility and film homogeneity were substantially poorer for the untreated silicon substrates. The stannoxane−substrate interaction potential is clearly particularly sensitive to minor modifications in silicon surface chemistry.

B. Synchrotron Radiation Spectroscopy of Organostannoxane Thin Films. The morphology of the organostannoxane thin film used for the SR-based measurements is shown in the inset to Figure 6. Note that, as for the dewetting studies described in section III.A, the film structure is cellular in nature and thus exposes a substantial amount of the underlying silicon substrate. This, coupled with the presence of adventitious carbon on the silicon substrates and the strong oxygen-derived photoemission signal from the SiO_2 layer make reliable analysis and interpretation of C 1s and O 1s spectra from the organostannoxane film extremely difficult. We have therefore focused on the acquisition of Fe- and Sn-derived core-level photoemission and RESPES spectra (as these signals arise solely from the adsorbed stannoxane clusters).

Valence band spectra ($h\nu = 60$ eV) taken from a silicon sample with and without an adsorbed organostannoxane layer are shown in Figure 6. Although it is clear that the overall shape of the spectrum changes little when the stannoxane overlayer is present (being dominated by the substrate valence band structure), an additional peak at a binding energy of 2 eV is observed. While this peak derives from the highest occupied molecular orbital (HOMO) of the stannoxane cluster, the spectrum shown in Figure 6b yields little information beyond the energetic position of the HOMO below the Fermi level. This is because with conventional photoemission it is extremely difficult − in the absence of a priori knowledge − to identify the electronic character of the peaks in a valence band spectrum. We have, therefore, used RESPES to probe the contribution of Fe and Sn to the frontier orbitals of the adsorbed stannoxane cluster.

RESPES[29] exploits the resonant enhancement of the spectral intensity of valence states associated with a particular chemical element. This occurs when the incoming photon energy is tuned to the absorption threshold of a more strongly bound core-level of that element. In this way, one gains insight into the partial density of states. This process is sketched in Figure 7a. Following threshold excitation of a core-level electron (in this case, from an Fe 2p level) into the unoccupied (Fe 3d-derived) density of states, nonradiant decay of an Fe 3d valence electron to the Fe 2p core-hole is accompanied by the emission of the originally excited core-level electron. Importantly, this process produces a single hole final state that is identical to that associated with direct valence band photoemission (as depicted in Figure 7b). Constructive interference between the two excitation channels leads to resonant enhancement of the spectral intensity of Fe 3d-related features in the valence band. RESPES therefore provides us with an element-specific, localized probe.

(28) The experiment was repeated many times with a number of samples prepared in an identical manner. The morphological variations observed as a function of position on the sample were comparable from sample to sample for H_2SO_4:H_2O_2-treated silicon substrates. Substantially higher levels of film inhomogeneity and sample irreproducibility were observed for substrates that were simply solvent-rinsed.

(29) See, for example: Nilsson, A. *J. Electron Spectrosc. Relat. Phenom.* **2002**, *126*, 3.

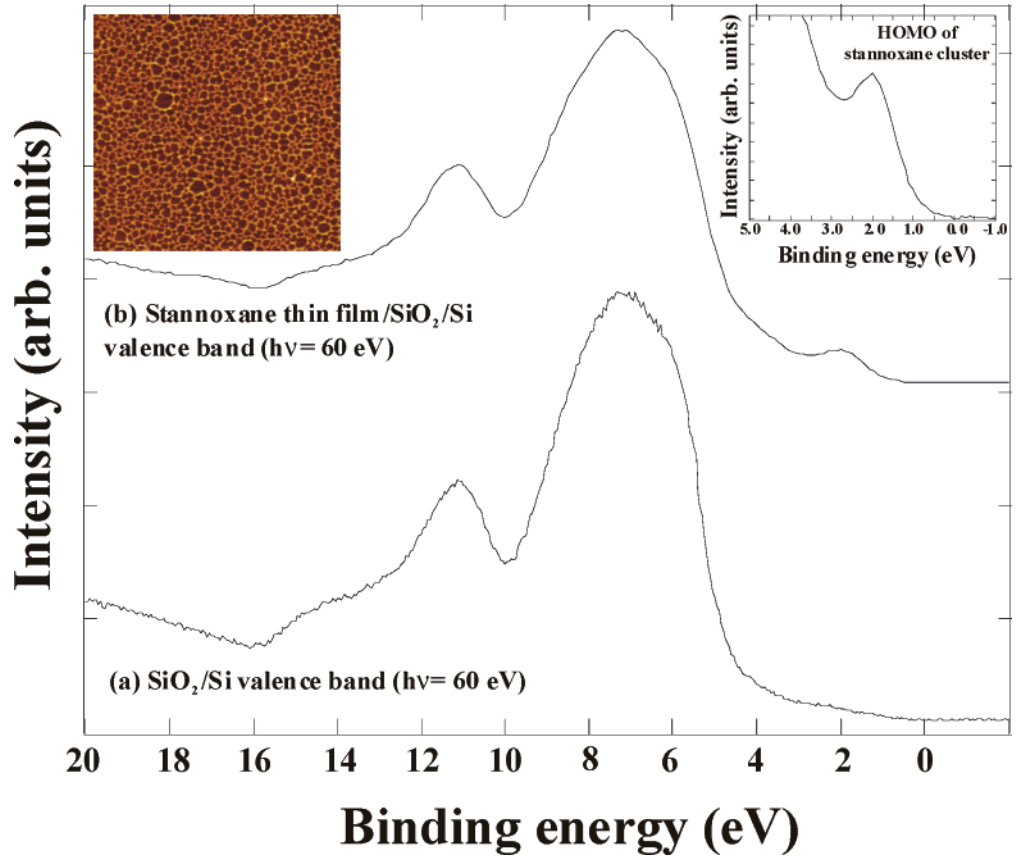

Figure 6. Valence band spectra for (a) native oxide-terminated Si(111) substrate, and (b) a thin organostannoxane film on the SiO_2/Si(111) substrate. Note that, although the substrate valence band structure dominates the spectrum in each case, the highest occupied molecular orbital (HOMO)-derived peak of the stannoxane film is visible in (b). (See also the inset on the right-hand side of the figure). Inset on left: AFM image (8 μm × 8 μm) of stannoxane film used for photoemission measurements.

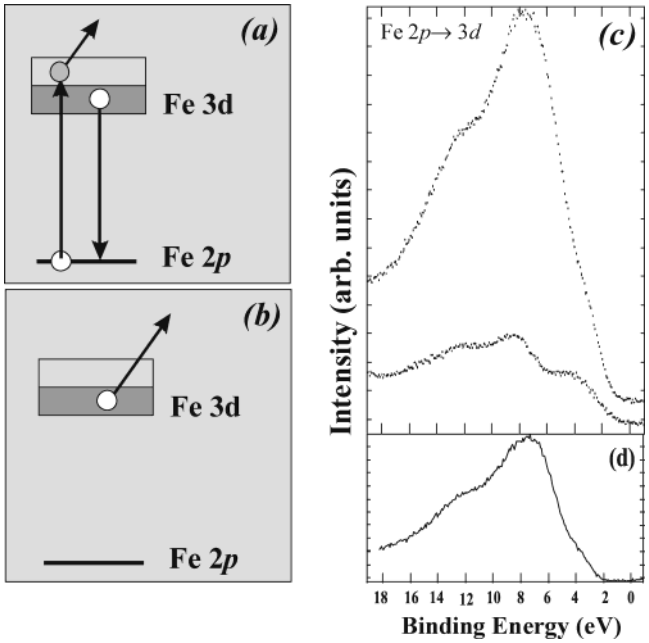

Figure 7. (a,b) Schematic illustrations of the resonant photoemission process for Fe 2p → 3d RESPES (see text for details). (c) On-resonance (upper spectrum) and off-resonance (lower spectrum) valence band spectra taken at photon energies of 711 and 702 eV, respectively. (d) On-resonance−off-resonance difference spectrum.

Valence band spectra from the organostannoxane−SiO_2/Si sample for photon energies of 702 and 711 eV are shown in Figure 7c. Below the Fe 2p threshold ($h\nu = 702$ eV), the spectra are dominated by photoemission from the SiO_2/Si substrate (compare the off-resonance spectra shown in Figures 7 and 8). As the photon energy is increased toward the Fe 2p threshold, the Fe 3d states are enhanced in the photoemission spectrum. By subtracting the off-resonance spectrum from the on-resonance spectrum, as shown in Figure 7d, the Fe 3d-derived partial density of states may be extracted. Three broad features are identified in the difference spectrum shown in Figure 7d: a shoulder at a binding energy of approximately 4 eV, an intense peak at 7.0 eV, and another shoulder at ∼11 eV. (Note that the combined photon and electron energy resolution for the Fe 2p → 3d RESPES measurements shown in Figure 7 was rather poor (>1 eV) due largely to the use of an analyzer pass energy of 90 eV to ensure sufficiently high electron count rates.)

It is now instructive to compare the Fe 2p → 3d RESPES difference spectrum shown in Figure 7c with the calculated and experimentally measured density of states of ferrocene, the "parent" molecule of the ferrocenyl groups at the periphery of the organostannoxane cluster (see Figure 1). A previous photoemission study[30] of adsorbed ferrocene identified a series of peaks at energies of ∼2.3, 4.4, 7.9, 12.3, and 17.2 eV with respect to the Fermi level. Through comparison with ground-state theoretical calculations for ferrocene, the various peaks were assigned to their corresponding orbitals. Of particular relevance to the present study, however, Dowben et al.[31] have discussed the enhancement of the ferrocene molecular orbital-

(30) Driscoll, D. C.; Dowben, P. A.; Boag, N. M.; Grade, M.; Barfuss, S. *J. Chem. Phys.* **1986**, *85*, 4802.
(31) Dowben, P. A.; Waldfried, C.; Komesu, T.; Welipitiya, D.; McAvoy, T.; Vescovo, E. *Chem. Phys. Lett.* **1998**, *283*, 44.

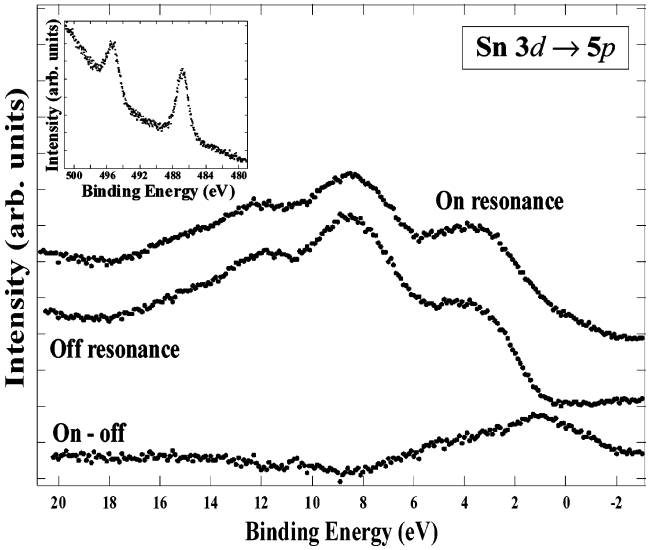

Figure 8. Sn 3d → 5p RESPES spectra. The "on-resonance" and "off-resonance" spectra were taken at photon energies of 488 and 480 eV, respectively. Note that the energy resolution is poor (≫1 eV fwhm), which leads to a substantial overestimate of the density of states at the Fermi level (binding energy = 0 eV). Nevertheless, the data clearly show that there is a substantially stronger contribution of Sn states (as compared to Fe states) to the higher lying occupied molecular orbitals. Inset: Sn 3d core-level photoemission spectrum ($h\nu = 550$ eV).

derived photoemission features in RESPES. They point out that the $4e_{1g}$, $7a_{1g}$, $6e_{1u}$, and $2e_{1g}$ features (at binding energies of ∼7.0, 10.9, and ∼13 eV) derive from molecular orbitals which have the highest level of π-Cp ligand orbital hybridization to Fe d states. The $8a_{1g}$ and $4e_{2g}$ molecular orbitals with binding energies of 4−5 eV and ∼4 eV, respectively, have strong localized Fe 3d character. Specifically, the $8a_{1g}$ and $4e_{2g}$ features arise from d_{z^2} and d_{xy},$d_{x^2-y^2}$ orbitals, respectively.

In Fe 2p → 3d RESPES, we should expect to observe strong enhancement of the photoemission features which arise from molecular orbitals having a large component of localized Fe 3d character. That intense resonances at ∼4 and ∼7 eV are observed in the difference spectrum shown in Figure 7c is strongly suggestive that these peaks derive from molecular orbitals with Fe 3d content similar to that of the $8a_{1g}$, $4e_{2g}$, and $4e_{1g}$ orbitals of the "parent" ferrocene molecule. The shoulder observed at an energy of ∼11 eV in Figure 6b must also arise from orbitals with a high degree of Fe d character, and a family of orbitals ($3e_{2u}$, $3e_{2g}$, $3e_{1g}$, $5e_{1u}$, and $7a_{1g}$) have previously been identified as contributing to this spectral feature in studies of ferrocene adsorption on Ag(100).[32]

It therefore appears that the ferrocenyl groups at the periphery of the stannoxane cluster retain a high degree of the electronic character of the ferrocene molecule. What is particularly interesting, however, is that with Fe 2p → 3d RESPES we find no evidence for a strong resonant enhancement of the HOMO-derived peak centered at ∼2 eV below the Fermi edge (see Figure 6b). This suggests that the highest occupied orbital is associated with very little (localized) Fe 3d character. A RESPES measurement involving photon energies crossing the Sn 3d edge was therefore carried out to probe whether Sn 5p states make a significant contribution to the HOMO of the stannoxane cluster. (The Sn 3d core-level photoemission spectrum is shown as an inset to Figure 8. Note that we expect a less intense resonant enhancement for the Sn 3d → 5p RESPES than for the Fe 3d-related RESPES measurements as the electric dipole transition from a state of orbital angular momentum l to an $l - 1$ state is much weaker than $l \rightarrow l + 1$.)

It is clear from Figure 8 that there is measurable resonant enhancement of the valence band in the near-Fermi level region when the photon energy is tuned to the Sn 3d threshold ($h\nu = 488$ eV). The apparent very high density of states at the Fermi level (0 binding energy) is a consequence of the poor energy resolution of the measurement and the associated high degree of broadening of the resonance structure. Notwithstanding the low energy resolution, however, the stronger contribution of the Sn partial density of states to the highest-lying molecular orbitals of the stannoxane complex is readily apparent from Figure 8. (In addition, a strong (and trivial) resonant enhancement of the HOMO feature − and the entire valence band spectrum − was observed for photon energies comparable to that of the C K edge (285 eV).)

IV. Conclusions

We have shown that organostannoxane thin films spin-cast onto native oxide-terminated silicon substrates dewet via a mechanism which leads to the formation of a cellular network having a high degree of spatial correlation in the dewetting centers. While the lack of film stability has important implications for the synthesis of high-quality organostannoxane layers on silicon substrates, the influence of a dewetting process with a well-defined correlation length opens up a number of possibilities related to patterning stannoxane (and other organometallic) thin films at the submicron and nanometer scale levels. In addition, given that a previous application of Minkowski functionals to polymer film stability called into question the presence of spatially correlated dewetting centers,[20] our quantitative analysis represents an important confirmation of morphological deviations from Poisson statistics in a molecular, nonpolymeric thin film. However, although it is tempting to associate the spatial correlations we observe with spinodal dewetting, we stress that early-stage coalescence of Poisson-distributed dewetting holes may also yield a spatial correlation length.[23]

Synchrotron radiation RESPES measurements have shown that the ferrocenyl groups at the periphery of the stannoxane cluster retain a high degree of ferrocene-like electronic character but that there is little Fe 3d contribution to the highest occupied molecular orbital. Instead, Sn 3d → 5p RESPES data highlight the role of Sn-derived states in determining the character of the higher-lying occupied frontier orbitals. Although our RESPES data provide a first insight into the electronic structure of this novel and complex organometallic cluster, a detailed theoretical study (combined with more comprehensive photoemission work) is required to elucidate fully the molecular orbital configuration.

Acknowledgment. This research has been supported by a Marie Curie fellowship (held by F.F.) of the European Community program "Human Potential" under contract number HPMT-CT-2001-00407. In addition, this work was supported by a European Community 5th Framework Research Training and Mobility grant: "Supramolecular Self-Assembly of Interfacial Nanostructures" (HPRN-CT-2002-00185). We also acknowledge the UK Engineering & Physical Sciences Research Council (EPSRC) for funding

(32) Welipitiya, D.; Dowben, P. A.; Zhang, J.; Pai, W. W.; Wendelken, J. F. *Surf. Sci.* **1996**, *367*, 20.

(under grant GR/01880/01), the Council for the Central Laboratory of the Research Councils (CCLRC) for the provision of beamtime at Daresbury SRS, and Enterprise Ireland for financial support under grant SC/2000/167. The beamtime experiments were facilitated by the expert technical assistance of George Miller, whom we sincerely thank. We also very gratefully acknowledge the assistance, expertise, and advice of V. R. Dhanak at Daresbury Lab.

LA036414Y